Journal of the Iranian Chemical Society (2020) 17:671–685
https://doi.org/10.1007/s13738-019-01805-0

ORIGINAL PAPER

Crystal structure, *Hirshfeld* surface analysis and theoretical calculations of an oxalato-bridged copper(II) complex: *μ*-oxalato-bis[(2,2′-bipyridine) hydrate copper(II) nitrate]

Zina Boutobba[1,2] · Amani Direm[1] · Koray Sayin[3] · Brahim El Bali[4] · Mohammed Lachkar[4] · Nourredine Benali-Cherif[5,6]

Received: 7 December 2018 / Accepted: 25 October 2019 / Published online: 5 November 2019

Abstract
The copper complex $[Cu_2(Bipy)_2(H_2O)_2(C_2O_4)(NO_3)_2]$ (Bipy = 2,2′-bipyridine; $C_2O_4^{2-}$ = oxalate) has been synthesized and characterized by single-crystal X-ray diffraction and FTIR spectroscopy. The structure determination revealed that the title compound contains centrosymmetric doubly charged dinuclear oxalato-bridged copper(II) complex cations, nitrate counter ions and water molecules. In this complex, the oxalate ligand is coordinated in a bis-bidentate bridging mode to the copper atoms. Each Cu(II) atom has a distorted tetragonal–bipyramidal environment, being coordinated by two N atoms of a chelating 2,2′-bipyridine ligand and two O atoms of the doubly deprotonated oxalate anion. Pairs of monodentate nitrate anions and aqua ligands are linked to the metallic cations in an axial position. The H-bonds occurring in the crystal structure result in the formation of 2D supramolecular chains and 3D networks. The *Hirshfeld* surface analysis of the complex has shown the presence of strong O–H…O and C–H…O hydrogen bonds together with non-classical weak C–H…*π*, *π*…*π*, *π*…*lp*/*lp*…*π* and *lp* …*lp* interactions. Furthermore, the theoretical calculations results are in agreement with the experimental geometric parameters. The NMR spectra and the MEP maps were also calculated.

Keywords Oxalato-bridged complexes · Crystal structure · Hydrogen bonds · *Hirshfeld* surface analysis · Theoretical calculation · MEP

Introduction

The ability of the oxalate anion to generate di- and polynuclear complexes is well known. The rich structural diversity of the oxalato-bridged complexes is due to the exceptional versatility of the oxalate ligand. Moreover, the oxalate bridge can efficiently mediate the exchange interactions between the paramagnetic metal ions, leading to interesting magnetic properties [1–4]. The magnetic interactions through the bridge depend markedly upon the coordinated ligands and the counter ions [5]. A great number of oxalato-bridged dinuclear complexes have been characterized so far [5–10]. These compounds are generally obtained through the reaction between a cationic complex having potentially free coordination sites and the oxalate anion. The construction of oxalate-containing homo- and hetero-metallics, which have applications as molecular-based magnetic materials, has enhanced the interest in the oxalato compounds.

We report herein the synthesis, the crystal structure and the computational studies, accomplished using the

✉ Amani Direm
amani_direm@yahoo.fr

1 Laboratory of Structures, Properties and Interatomic Interactions LASPI2A, Faculty of Sciences and Technology, University of "Abbes Laghrour", 40000 Khenchela, Algeria

2 Département de Chimie, Faculté des Sciences Exactes, des Sciences de la Nature et de la vie, Université "Larbi Ben M'hidi", 04000 Oum El Bouaghi, Algeria

3 Department of Chemistry, Faculty of Science, Cumhuriyet University, 58140 Sivas, Turkey

4 Laboratory of Engineering of Organometallic and Molecular Materials, "LIMOM" URAC 19, Department of Chemistry, Faculty of Sciences, PO Box 1796, 30000 Fès, Morocco

5 Ecole Nationale Polytechnique, 25000 Constantine, Algeria

6 Université de Bouira, Bouira, Algeria

HF/LANL2DZ level in gas phase, of the copper complex $[Cu_2(Bipy)_2(H_2O)_2(C_2O_4)(NO_3)_2]$ (Bipy = 2,2′-bipyridine; $C_2O_4^{2-}$ = oxalate). The dinuclear complex has been previously mentioned in the literature [11]. It was prepared by direct treatment of an aqueous solution of 2,2′-bipyridine with $Cu(NO_3)_2{\cdot}3H_2O$ in an aqueous solution, which was then added to an aqueous solution of $K_2C_2O_4{\cdot}H_2O$. Although the literature [11] has reported a different synthesis procedure and was dedicated to its crystal structure and magnetic properties, there is a lack of information on its optimized structure, geometric parameters, vibration frequencies, molecular electrostatic potential (MEP) maps, MEP contours and the nuclear magnetic resonance (NMR). Moreover, the *Hirshfeld* surface analysis of the intermolecular interactions within the title complex will be undertaken for the first time.

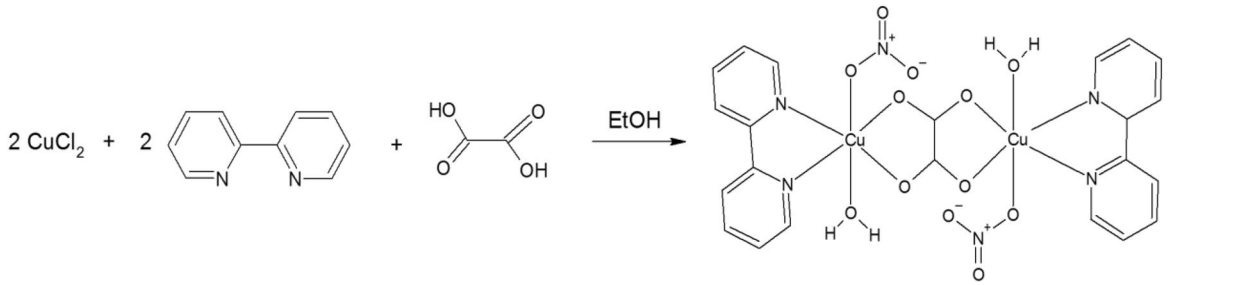

Experimental

Synthesis

The chemicals and solvents used in this work are of analytical grade and available commercially and were used without further purification. $CuCl_2{\cdot}2H_2O$ (0.341 g, 2 mmol) and 2,2′-bipyridine (0.312 g, 2 mmol) were dissolved in ethanol (10 mL), and a solution of oxalic acid (0.09 g, 1 mmol in 10 mL of ethanol) was then added dropwise to the obtained mixture, in a 2:2:1 ratio. After slowly adding nitric acid (10 mL), the resulting solution was stirred at room temperature for 30 min until an almost clear solution was obtained and allowed to stand at room temperature after filtration of any amount of insoluble material. Blue block-like crystals suitable for X-ray analysis appeared after a few days.

Table 1 Experimental details of the data collection strategy

Diffractometer	Oxford diffraction Xcalibur
Wavelength (Mo Kα), Å	0.71073
2θ range for data collection (°)	
θ_{max}	29.27°
θ_{min}	3.17°
Measured reflections	12,922
Independent reflections	3096
Reflections with $I > 2\sigma(I)$	2777
R_{int}	0.0289
Limiting indices	
h	−10 → 10
k	−13 → 14
l	−21 → 22

Crystal structure analysis

A dark blue block-like crystal of (0.10 × 0.15 × 0.15 mm) sizes was selected for the structural analysis. Diffraction data were collected at room temperature and obtained with an Oxford automatic four-circle diffractometer using graphite-monochromated MoK_α radiation (λ = 0.71073Å) and operating with the ω–θ scan mode. The complete data collection strategy is summarized in Table 1.

The unit cell determination and data reduction were performed using the *CrysAlis* program suite [12] on the full set of data. The integration of the data using a monoclinic unit cell yielded a total of 12,922 reflections to a maximum θ angle of 29.27°, of which 3410 were independent and 2777 were greater than $2\sigma(I)$. The structure was solved by direct method using the *SIR*2004 program [13] and refined by full-matrix least-squares on F^2 including all reflections with *SHELXL*-2016 [14]. Crystal parameters and refinement results are summarized in Table 2.

All non-hydrogen atoms were anisotropically refined. All hydrogen atoms were located on difference Fourier maps. The aromatic ones were then fixed in calculated positions with distances constraints of C–H = 0.93 Å [U_{iso}(H) = 1.2U_{eq}(C)] except for water hydrogens which were clearly visible in difference maps and fixed with U_{iso}(H) = 1.5 U_{eq}(O). The refinements converged at conventional R factor of 0.0368 (for 2777 reflections with $I \geq 2\sigma(I)$) and wR of 9.07%. Maximum and minimum peaks in the final difference Fourier syntheses were 0.686 and − 0.519 e $Å^{-3}$. All calculations were performed using the *WinGX* crystallographic software package [15]. Structural representations of the title

Table 2 Crystal data and structure refinement of the title complex

Crystal data	
Empirical formula	$C_{11}H_{10}CuN_3O_6$
Formula weight (g mol^{-1})	$M_r = 343.77$
Temperature (K)	293
Crystal system	Monoclinic
Space group	$P2_1/n$
Unit cell dimensions (Å, °)	
a	7.6587(3)
b	10.2273(4)
c	16.1551(6)
β	99.583(4)
Volume (Å^3)	1247.74(8)
Z	4
Calculated density (g/cm^3)	1.830
Absorption coefficient (mm^{-1})	1.785
$F(000)$	696
Crystal size (mm^3)	0.10×0.15×0.15
Color	Dark blue
Shape	Block-like crystal
Cell parameters from	2777 reflections
Refinement	
Least-squares matrix	Full
Final R indices [$F^2 > 2\sigma(F^2)$]	
R_1	0.0368
wR_2	0.0907
R indices (all data)	
R_1	0.0425
wR_2	0.0940
Goodness-of-fit on F^2	1.166
Data/restraints/parameters	3410/0/190
Largest difference peak and hole (e A^{-3})	
$\Delta\rho_{max}$	0.686 e Å^{-3}
$\Delta\rho_{min}$	−0.519 e Å^{-3}

compound were drawn using ORTEP-3 [16] and MERCURY [17]. Analyses were carried out using the program PLATON [18], as incorporated in the *WinGX* [15] suite. According to the data obtained, the unit cell parameters are comparable to the previous results [11]. The crystal structure is, however, determined with a lower R value (0.0368) compared to the previously published study (0.040).

Further details on the crystal structure investigations of complex may be obtained from the Cambridge Crystallographic Data Centre, CCDC, 12 Union Road, Cambridge CB2 1EZ, UK [Email: de-posit@ccdc.cam.ac.uk; http://www.ccdc.cam.ac.uk/deposit], on quoting the depository number CCDC-1578572.

Spectroscopic measurements

The FTIR spectrum has been recorded by a KBr pellet technique in the frequency region from 400 to 4000 cm^{-1}, using a PerkinElmer Spectrum GX spectrometer.

Computational details

The computational investigations of mentioned complex are performed by *Gaussian* programs; namely *GaussView* 5.0.9 [19] and *Gaussian* 09 AS64L-G09RevD.01 [20]. Furthermore, preparation of figures was done by means of *ChemBioDraw Ultra* Version (13.0.0.3015) [21]. It is reported that HF method has advantages in the determination of electronic properties of molecule [22]. Therefore, HF is the first ab initio method, it was used in calculations, and LANL2DZ was selected as the basis set. The studied complex is dinuclear. The number of electrons in the compound examined is quite high. A more basic level of the LANL2DZ basis set was chosen for both the high number of electrons and the comparison of the results with the experimental results in general. It is known that 10 core electrons were neglected in LANL2DZ basis set. The selected method and the base set are sufficient for comparison of experimental results and were used in many articles [23–25]. In calculation results, no imaginary frequency was observed. Additionally, GIAO method was used as additional method for NMR calculations. Tetramethylsilane was used as reference substance in calculation of chemical shift values of carbon and hydrogen atoms.

Results and discussion

Crystal structure

The title compound is a binuclear complex, formed by two molecule's halves, which are related by a crystallographic inversion centre situated in the middle of the oxalate bridge (Fig. 1). The structure of the complex consists of two Cu^{II} ions as central atoms possessing a distorted tetragonal–bipyramidal geometry. The four equatorial positions, for each metallic centre, are occupied by two N atoms belonging to the bidentately coordinated 2,2′-bipyridine molecules [Cu–N = 1.984(2) and 1.969(2)Å] and two O atoms from the tetradentate oxalate anion [Cu–O = 1.966(2) and 1.991(2) Å]. These atoms define the equatorial plane with a maximum deviation from the least-squares plane of 0.038 Å. The Cu–N_{bipy} (average, 1.976(2) Å) and Cu–O_{ox} (average, 1.978(2) Å) bond distances are comparable to those observed in other six-coordinated complexes where the copper ion is bounded to 2,2′-bipyridine: Cu(4,4′-$(C(CH_3)_3)_2$-2,2′-bipyridine)$(NO_3)_2$ [Cu–N, 1.965(2) and 1.980(2) Å] [26],

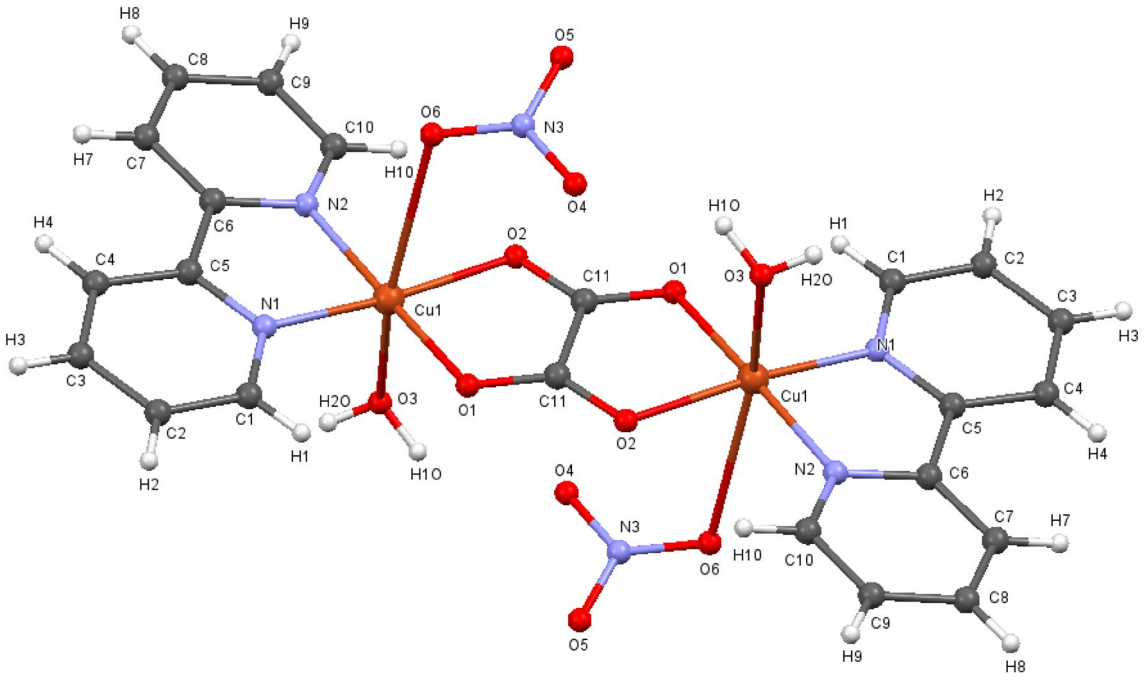

Fig. 1 A molecular drawing of the title compound showing the atomic labels

or oxalate bridges: $[Cu_2(Oxalate)_2(pyrazine)_3]_n$ [Cu–O, 1.982(6) and 1.981(6) Å] [27].

The axial coordination sites are occupied by two oxygen atoms, one of them belongs to the water molecule and the other to the nitrate counter ion. The first axial Cu1–O3 distance of 2.311(2) Å is in agreement with that found in similar reported Cu–Ow bonds [28, 29]. The difference between it and the equatorial bond length (a difference of 0.33 Å) is slightly longer than those observed in other six-coordinated copper(II) complexes [30]. However, the nitrate counter ion is weakly bonded to the copper(II) centre in the second apical position, with a Cu–O bond distance markedly longer than the equatorial ones [Cu1–O6 = 2.763(2) Å], due to the Jahn–Teller effect. This value is similar to those reported for the related nitrate copper(II) complexes $[Cu(NO_3)(C_{10}H_8N_2)(H_2O)_3(NO_3)]$ (2.624(2) Å) [31]. The short Cu–Cu distance through the oxalate of 5.157(2) Å is similar to the one observed in [11] (5.143 Å) and slightly shorter than the intermetallic separation observed in a related μ-oxalato-bridged dicopper complex with 2,2′-bipyridine perchlorate dimethylformamide disolvate monohydrate (5.6032(9) Å) [32]. This does not exclude possible antiferromagnetic interactions, through super exchange process mediating the oxalate O–C–O and O–C–C–O bridges, as the case in the dinuclear copper complex $[Cu_2(bpy)_2(\mu\text{-ox})]^{2+}$ (d_{Cu-Cu} = 5.134 Å) [33].

The 2,2′-bipyridine ligand has a slightly twisted geometry and each ring–ring stacked pair defines an inter-planar dihedral angle of 5.68°. The C–N and C–C bond lengths within this ligand are normal for bipyridine derivatives [34–36]. The centroid–centroid distance between two bipyridine stacked rings is 7.659 Å. The structural parameters of the oxalate bridge are comparable with those previously observed in such metal-coordinated groups. The oxalate group is nearly planar (the largest deviation of atoms from the mean plane is 0.023 Å) with a long C–C bond length of 1.550(2) Å. Furthermore, the torsion angle within the oxalate ligand, O1–C11–C11–O2, has the value of 0.4(3)°. In addition, the dihedral angle between the mean oxalate plane and the mean bipyridine plane is 9.58°. Some of the most relevant interatomic bond distances are listed in Table 3.

Table 3 Selected bond lengths (Å) for $[Cu_2(Bipy)_2(H_2O)_2(C_2O_4)](NO_3)_2$

Selected bond lengths		
Cu1	O1	1.9664(17)
Cu1	N2	1.969(2)
Cu1	N1	1.984(2)
Cu1	O2	1.9913(16)
Cu1	O3	2.3108(18)
Cu1	O6	2.763(2)
O2	$C11^{i}$	1.250(3)
O1	C11	1.259(3)
O4	N3	1.255(3)
O5	N3	1.258(3)
O6	N3	1.250(3)

Symmetry codes: (i) 2 − *x*, − *y*, 1 − *z*

Table 4 Hydrogen bond lengths (Å) and angles (°)

D-H…A	*D-H*	*H…A*	*D…A*	*D-H…A*
Intramolecular interactions				
O3–H1O…O4$^{(i)}$	0.86	2.14	2.871(3)	142
C1–H1…O1	0.93	2.58	3.090(3)	115
Intermolecular interactions				
O3–H2O…O5$^{(ii)}$	0.81	2.03	2.781(2)	155
C2–H2…O5$^{(iii)}$	0.93	2.59	3.508(3)	170
C2–H2…O6$^{(iii)}$	0.93	2.51	3.266(3)	139
C4–H4…O4$^{(iv)}$	0.93	2.48	3.409(3)	176
C7–H7…O4$^{(iv)}$	0.93	2.56	3.489(3)	178
C7–H7…O6$^{(iv)}$	0.93	2.42	3.105(3)	131
C9–H9…O5$^{(v)}$	0.93	2.53	3.230(3)	132
C9–H9…O2$^{(v)}$	0.93	2.63	3.460(3)	149
C10–H10…O2	0.93	2.65	3.153(3)	115

Symmetry codes: (i) 2 − *x*, − *y*, 1 − *z*;(ii) − 1+*x*, *y*, *z*;(iii) 3/2 − *x*,–½ +*y*, ½ − *z*;(iv) 3/2 − *x*, ½ +*y*, ½ − *z*;(v) 2 − *x*, 1 –*y*, 1 − *z*

The coordinated water molecules of this complex are *trans* to each other. Each one of them is doubly hydrogen-bonded (Table 4) to an O atom of the nitrate counter ion, yielding to an intramolecular contact on the one hand (2.871(2) Å) and to another counter ion's oxygen belonging to a second molecule (2.781(2) Å) on the other hand (Fig. 2).

In the crystal packing, the neighboring molecules are linked to each other through intermolecular Ow–Hw···O_{NO3-} hydrogen bonds into a C(6) one-dimensional infinite chain disposed parallel to the (*ac*) plane. Each couple of intra- and intermolecular hydrogen bonds takes part in forming water–nitrate twelve-membered cycles with the graph-set descriptors $R_2^2(12)$ and $R_4^4(12)$ [37] (Fig. 3).

Each couple of intra- and intermolecular hydrogen bonds takes part in forming water–nitrate twelve-membered cycles. It is noteworthy that the twelve-membered clusters, delineated through these H-bonds, form a 2D structure as shown

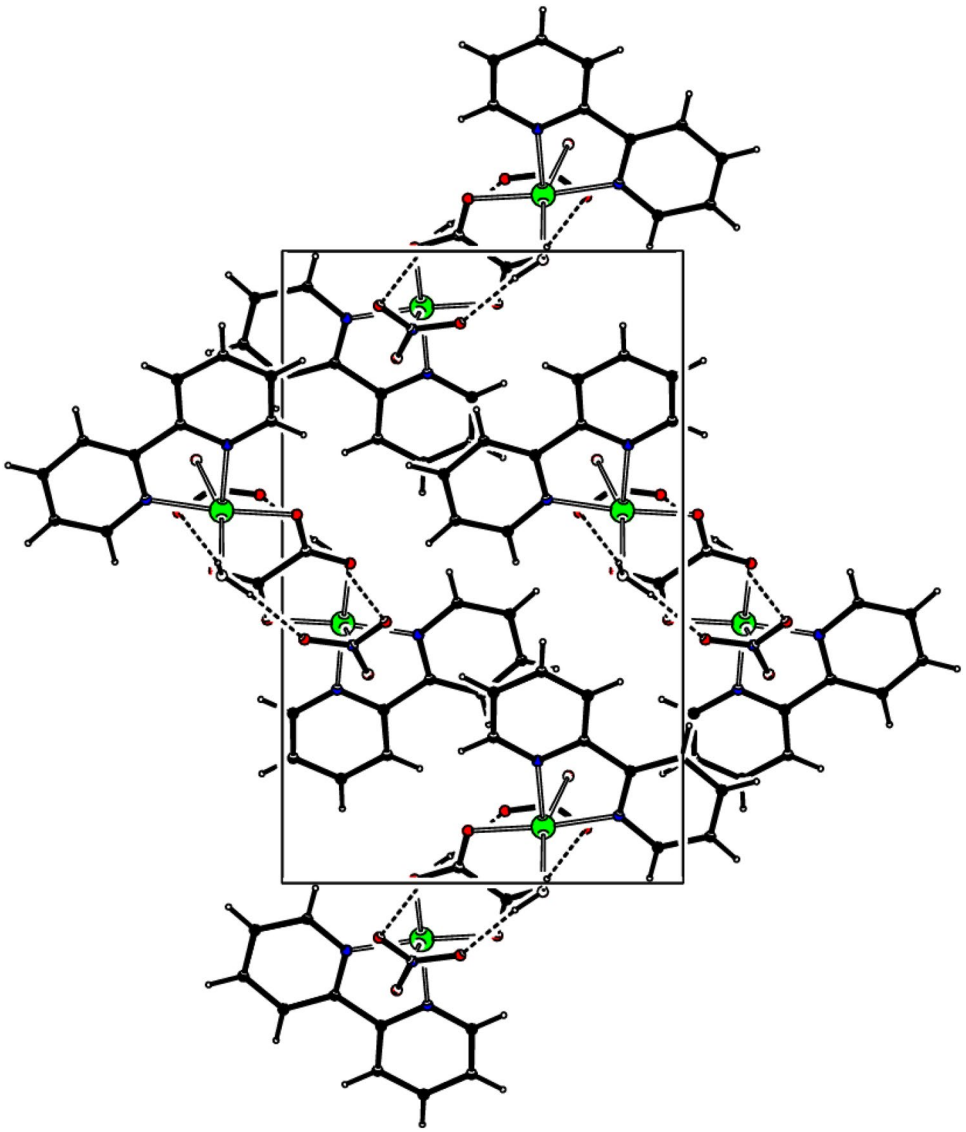

Fig. 2 Crystal packing of the title compound showing the H-bonding patterns

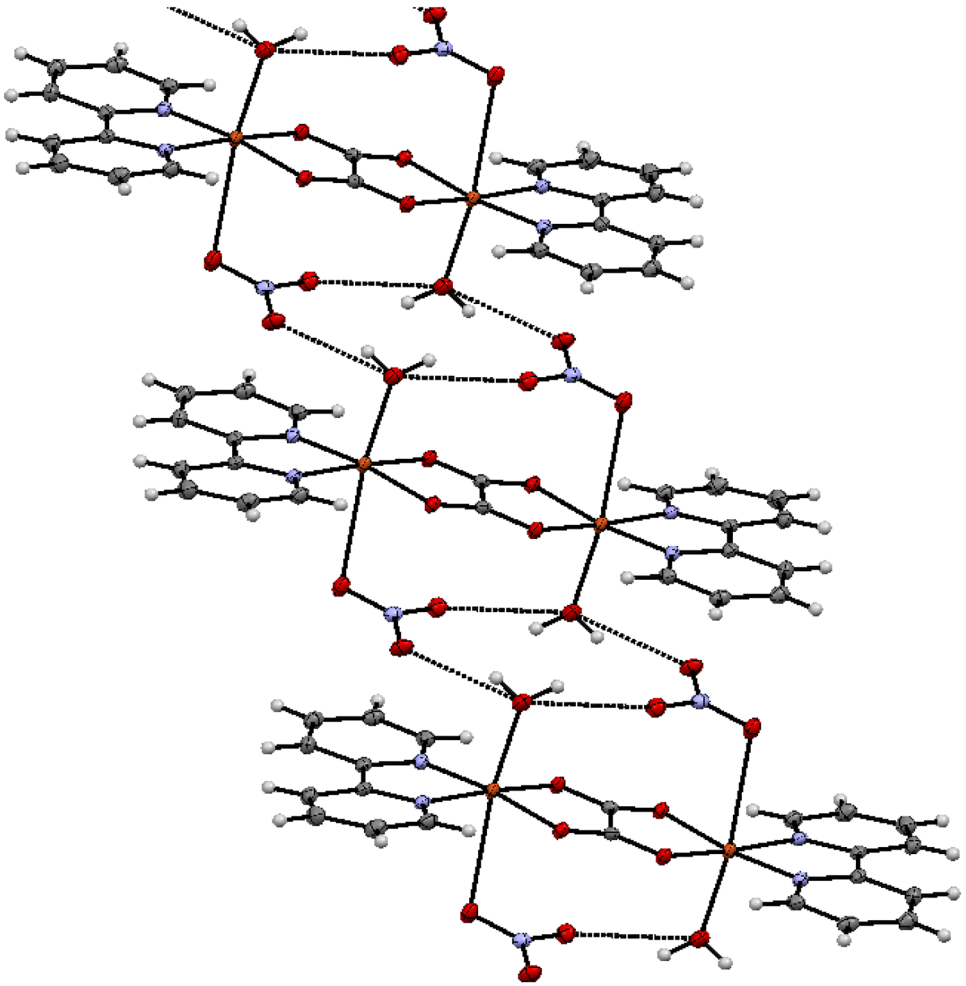

Fig. 3 C(6) infinite chains and R(12) cycles created by intra- and intermolecular interactions

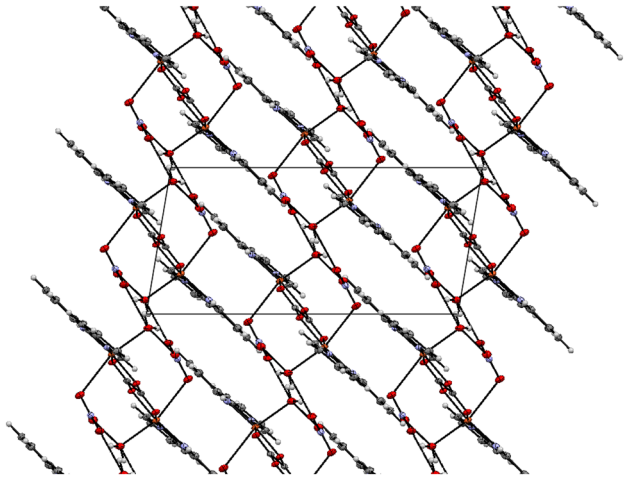

Fig. 4 Projection of the crystal packing in the (*ac*) plane showing the polymeric layers formed with Ow—Hw···O_{NO3-} H-bonds

in Fig. 4. The same 2D H-bonds packing arrangement has been observed for the $[Cu_2(ox)(phen)_2(H_2O)_2(NO_3)_2]$ complex [38].

The crystal packing is stabilized by non-classical hydrogen bonds. The weak intra- and intermolecular interactions are of the C-H…O type. The O4 oxygen atom of the nitrate ion participates, as a proton acceptor, in a bifurcated intermolecular interaction involving the C4 and C7 carbon atoms from the 2,2′-bipyridine ligand. The distances C4…$O4^{(iv)}$ and C7…$O4^{(iv)}$ are 3.409(3) and 3.489(3) Å, respectively, and the hydrogen bonds are nearly linear (176° and 178°). The C2 atom is implicated in a three-centre hydrogen bond connecting the two nitrate oxygens O5 and O6 [3.508(3) and 3.266(3) Å, respectively]. The same nitrato counter-ion oxygens (O5 and O6) give rise to two bifurcated H-bonds with bipyridine C9 and C7 carbons, respectively [3.230(3) and 3.105(3) Å]. A weak intramolecular C–H…O_{Ox} of 3.090(3) Å has been observed between the oxalate bridges and the pyridyl rings.

Hirshfeld surface analysis

The *Hirshfeld* surface analysis has become a valuable tool for analyzing intermolecular interactions in a novel visual manner [39–41]. For each point on the *Hirshfeld* isosurface,

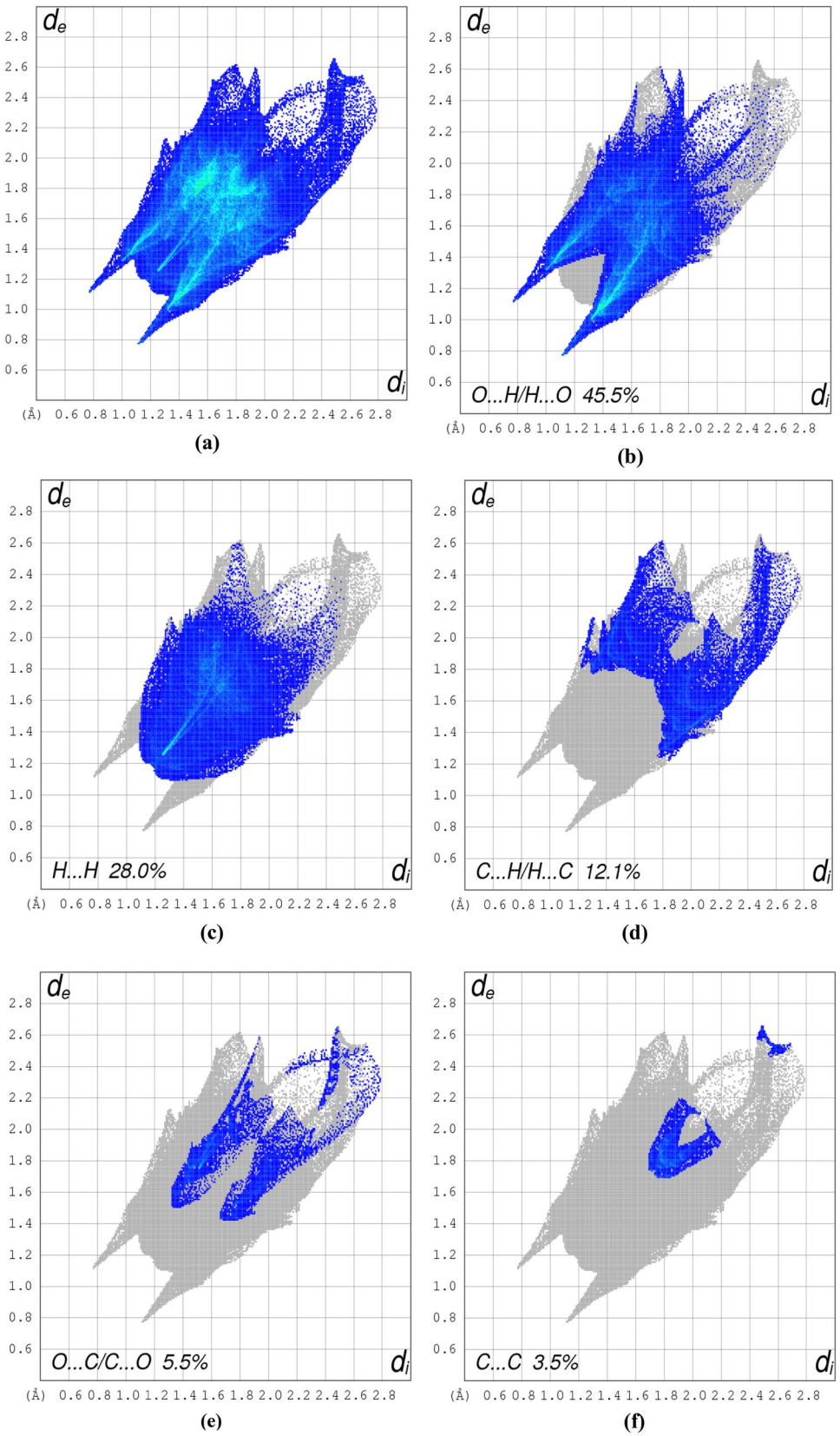

Fig. 5 Fingerprint plots of the title compound showing (a) the total contribution of all the interactions and decomposed fingerprint plots of the (b) O…H/H…O, (c) H…H, (d) C…H/H…C, (e) O…C/C…O, (f) C…C, (g) N…C/C…N, (h) N…H/H…N,(i) O…N/N…O, (j) O…O, (k) N…N contacts with their percentages

Fig. 5 (continued)

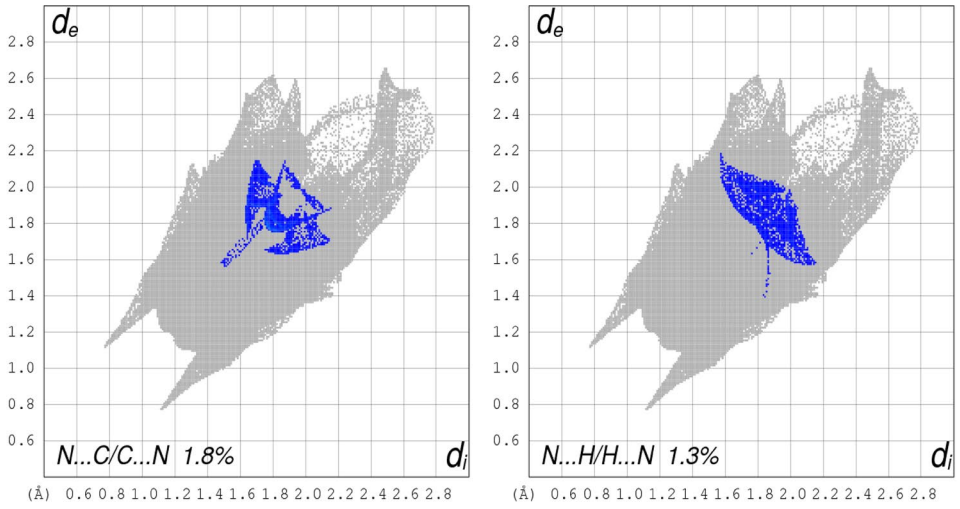

(g)

(h)

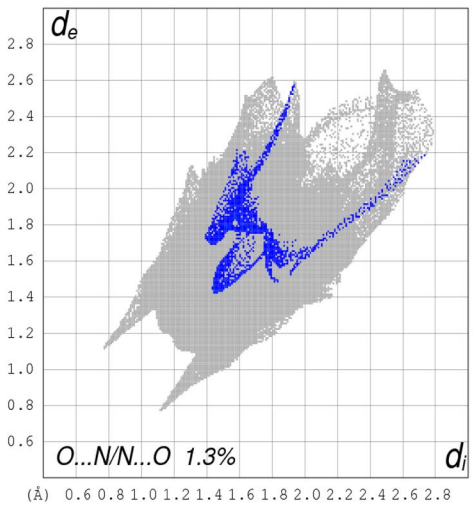

(i)

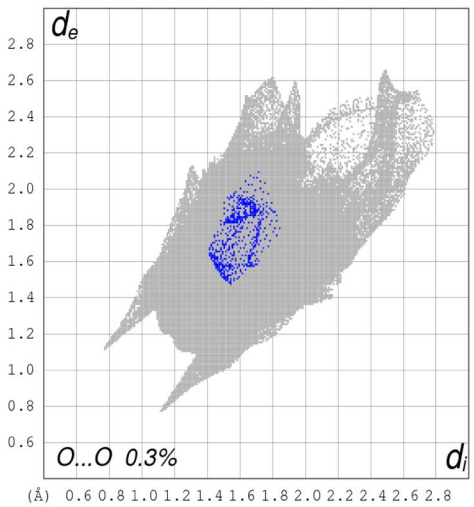

(j)

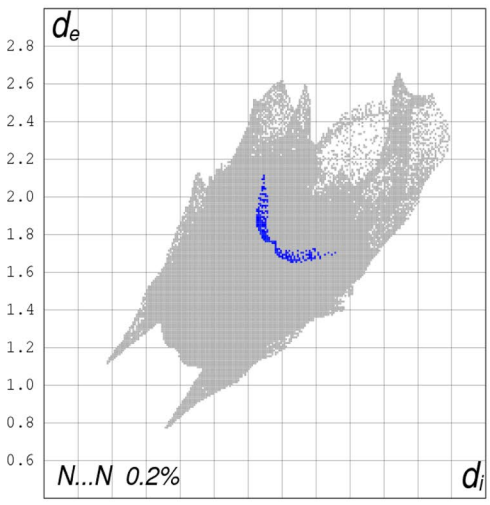

(k)

Scheme 1 Percentage contributions of the different intermolecular contacts to the *Hirshfeld* surface of the title compound

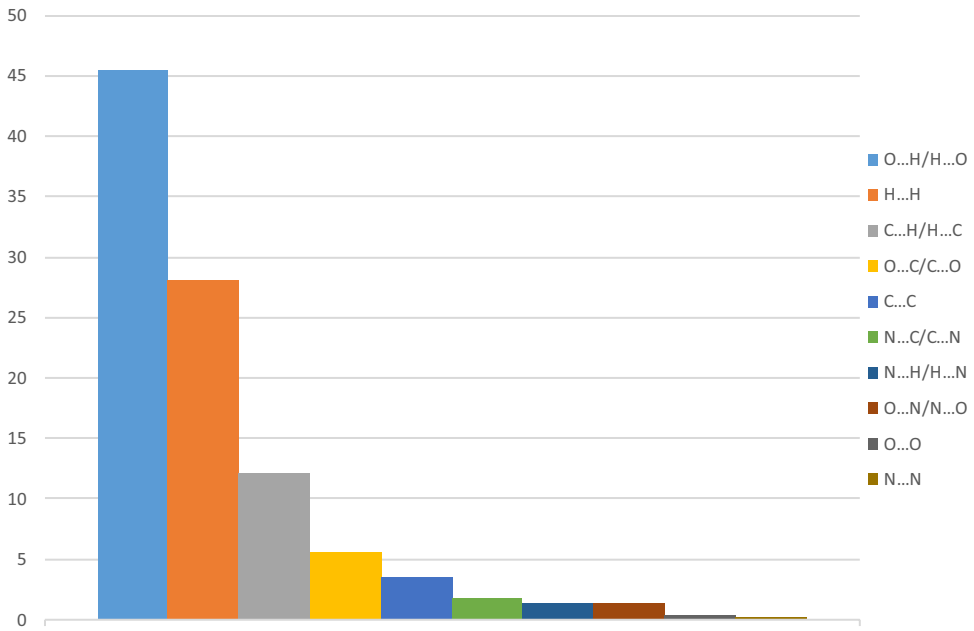

two distances are defined, namely d_e which is defined as the distance from the point to the nearest nucleus external to the surface and d_i described as the distance to the nearest nucleus internal to the surface. The normalized contact distance d_{norm} based on d_e and d_i is given by the following equation:

$$d_{norm} = \frac{d_i - r_i^{vdw}}{r_i^{vdw}} + \frac{d_e + r_e^{vdw}}{r_e^{vdw}}$$

where r_i^{vdw} and r_e^{vdw} are the van der Waals radii of the appropriate atoms which are internal and external to the surface, respectively. The value of d_{norm} is negative or positive when intermolecular contacts are shorter or longer than r^{vdW}, respectively. When d_{norm} is mapped on the *Hirshfeld* surface, close intermolecular distances are characterized by three colored regions: Red regions stand for closer contacts and negative d_{norm} value, blue regions represent longer contacts and positive d_{norm} value, and white regions correspond to the distance of contacts which is exactly equal to the *van der Waals* separation and with a d_{norm} value being equal to zero. The combination of d_e and d_i in the form of bi-dimensional histogram [42] affords a practical summary of the different intermolecular contacts in the crystal structure. All *Hirshfeld* surfaces and their associated 2D fingerprint plots (Fig. 5) were calculated using *Crystal Explorer* 3.1 software [43]. The contribution of the hydrogen bonds and the different non-classical contacts is given in Scheme 1.

As shown in Fig. 5 and Scheme 1, O…H/H…O (Fig. 5a), H…H (Fig. 5b) and C…H/H…C (Fig. 5c) contacts are the dominant contacts in the crystal structure of the title compound with a contribution to the whole *Hirshfeld* surface of 45.5%, 28.0% and 12.1%, respectively. These results, in the case of the O…H/H…O contacts, represented as two sharp spikes were considered as the most significant contributor, in the presence of shortest contacts at about ($d_e + d_i \sim 1.9$ ◆) which are associated with the interaction O3–H2O…O5 and its reciprocal O5…H2O–O3, highlighted in Fig. 6 as feature (1). This figure shows that the O…H/H…O contacts originate mainly from the C–H…O hydrogen bonds since the hydrogens of the title compounds are all related to carbons except for the case of the two water hydrogens.

Considered as the second most contributor to the total *Hirshfeld* surface around the molecule, the H…H contacts appearing as asymmetrically scattered points covering a large region of the two-dimensional fingerprint (Fig. 5c) exhibit a shortest contact of 2.34 ◆. The d_e representation mapped on the *Hirshfeld* surface indicates its origin: being the C9–H9…H10–C10 interaction and its reciprocal C10–H10…H9–C9, which are illustrated with (feature (2)) in Fig. 6b. Moreover, the O–H…H–C/C–H…H–O interactions have been observed to be involved in the H…H contacts.

The 12.1% contribution from the C…H/H…C contacts (Fig. 5d) to the *Hirshfeld* surface is generally slightly favored in C–H aromatic molecules. This results in a short contact at ($d_e + d_i \sim 3.0$ ◆) associated with the C7–H7…π interaction, pointed out with the feature (3) on the *shape index* function mapped on the total *Hirshfeld* area (Fig. 7) and represented as two blue and red triangles. In addition, the π…π stacking is present in this structure with a contribution of 3.5% (Fig. 5f); the shortest distance separating the mean planes through the 2,2-bipyridine ligands is 3.42 ◆ (feature (4) of Fig. 7).

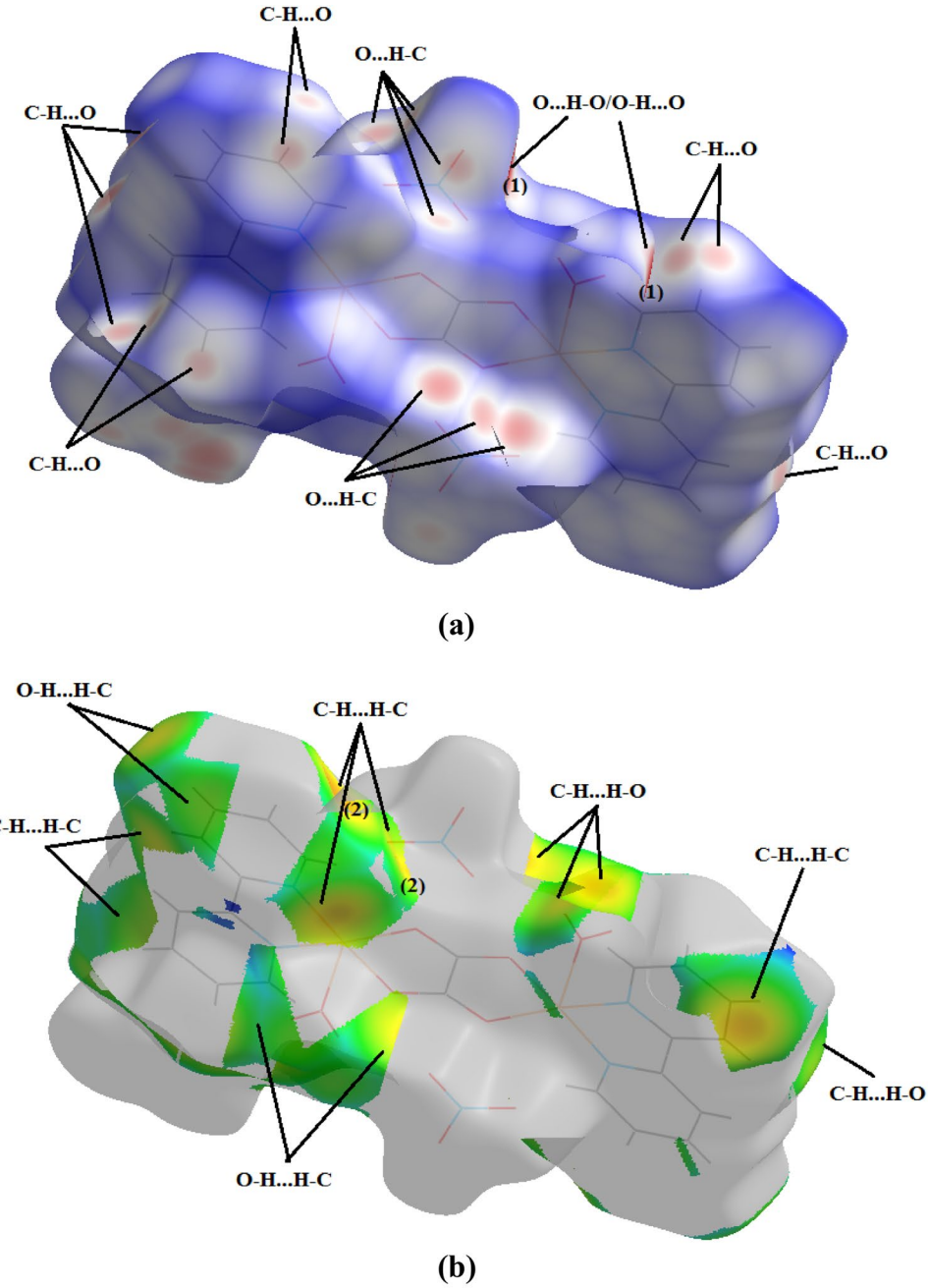

Fig. 6 (**a**) d_{norm} and (**b**) d_e representations mapped on the *Hirshfeld* surface of the molecule

Furthermore, *lp*…*π*/*π*…*lp* interactions were also observed as a result of the C…O/O…C and C…N/N…C contacts, with contributions of 5.5% (Fig. 5e) and 1.8% (Fig. 5g), respectively. Despite the small proportion of 1.3% (Fig. 5h), the crystal structure of the title compound consists of a short N…H/H…N contact at ($d_e + d_i \sim 3.22$ ♦), which could be attributed to the reciprocal C7–H7…N1/N1…H7–C7 interactions. Similarly, the *lp*…*lp* interactions resulting from the N…O/O…N, O…O and N…N contacts display a small contribution to the total *Hirshfeld* surface, being 1.3% (Fig 5i), 0.3% (Fig. 5j) and 0.2% (Fig. 5k), respectively.

Spectroscopic interpretation

Characteristic vibrations were observed for this complex; according to Nonoyama [5], the distinction between dimeric bridging complexes and chelating monomeric complexes lies in the position and the intensity of the carbonyl (C=O) vibrations. The FTIR spectra (Fig. 8) show characteristic bands of the oxalate bridging ligand [44–47], namely strong absorptions at 1634 and 1335 cm^{-1} attributed to the asymmetric and symmetric υ_{as}(C–O) and υ_s(C–O) stretchings. The bending of the δ(O–C–O) bond was observed at 825 cm^{-1}

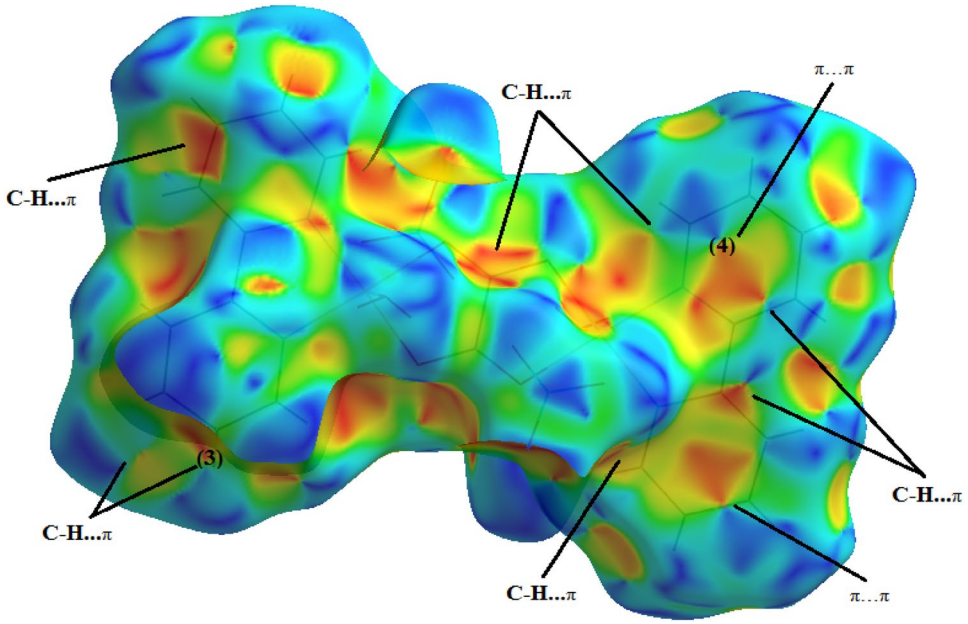

Fig. 7 *Shape index* representation showing the C-H…π and π…π interactions

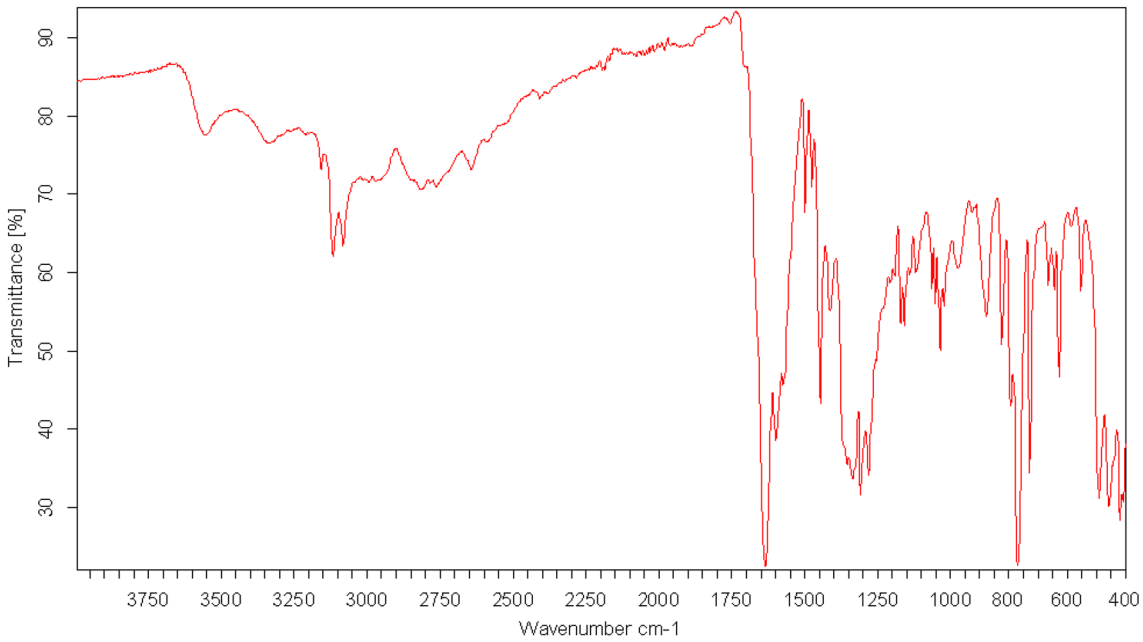

Fig. 8 FTIR spectrum of the title complex

[48, 49]. The appearance of Cu–O and Cu–N vibration bands in the 445–553 cm^{-1} region confirms the coordination of the oxalate ligand through its oxygens and the coordination of the bipyridine ligand through its nitrogens. The υ(C–C) and υ(C–N) stretching bands of the free 2,2-bipyridine ligand in the 1600–1400 cm^{-1} region are sensitive to chelation. These bands shift to higher frequencies in the complex (1599 and 1560 cm^{-1}), thus indicating the involvement of the 2,2-bipyridine nitrogens in the coordination with the copper(II) ions. The other characteristic vibrations of the free 2,2-bipyridine are the C–H out-of-plane deformations which appear as a strong band at 756 cm^{-1} and a weak satellite at 739 cm^{-1} [49]; upon chelation, two strong bands appear at ~ 770 and ~ 729 cm^{-1}, while the broad band at 3500 cm^{-1} is an indication of the coordinating water molecules. The IR spectrum exhibits stretching frequencies due to the nitrate counter ion coordinated in the expected unidentate bonding mode, namely $\upsilon(NO_3)$: 1445, 1355, 1300, 1010 cm^{-1} [50].

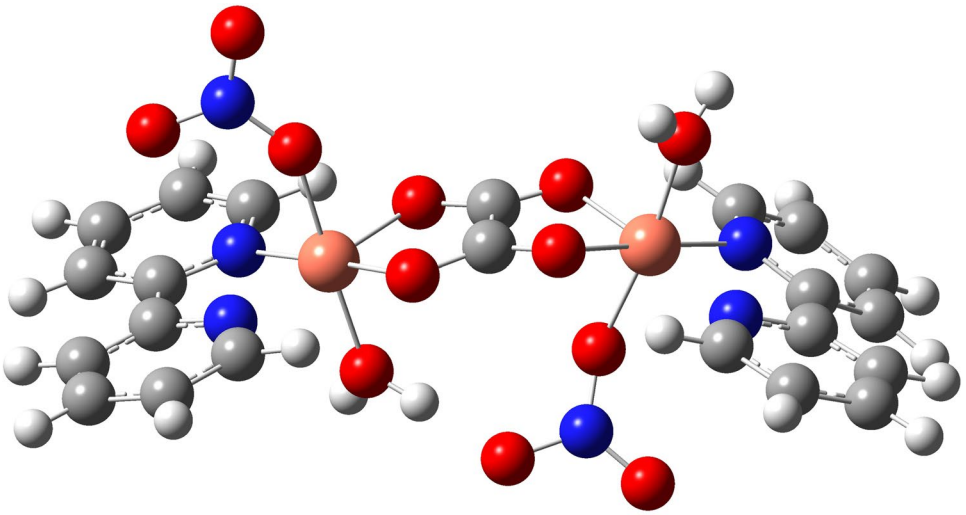

Fig. 9 Optimized structure of $[Cu_2(Bipy)_2(H_2O)_2(C_2O_4)](NO_3)_2$ at HF/LANL2DZ level

Table 5 Some experimental and calculated structural parameters obtained with the HF/6-31G(d) level in gas phase

	Experimental	Calculated
Bond lengths (Å)		
Cu1–O1	1.966	1.918
Cu1–N2	1.969	1.974
Cu1–N1	1.984	2.012
Cu1–O2	1.991	1.919
O2–C11	1.250	1.307
N1–C1	1.338	1.328
N1–C5	1.346	1.345
O6–N3	1.250	1.296
C5–C4	1.392	1.384
C5–C6	1.480	1.479
C9–C8	1.384	1.391
C9–C10	1.388	1.391
C4–C3	1.387	1.398
C2–C3	1.385	1.390
C2–C1	1.386	1.394
O1–C11	1.259	1.305
N2–C10	1.342	1.333
N2–C6	1.351	1.349
Bond angles (°)		
O1–Cu1–N2	173.94	177.32
O1–Cu1–N1	94.8	96.01
N2–Cu1–N1	82.34	81.33
O1–Cu1–O2	85.12	86.65
N2–Cu1–O2	97.00	96.00
N1–Cu1–O2	172.33	177.32
O1–Cu1–O3	96.06	88.38
N2–Cu1–O3	89.77	91.27
N1–Cu1–O3	102.03	90.31
O2–Cu1–O3	85.59	90.04

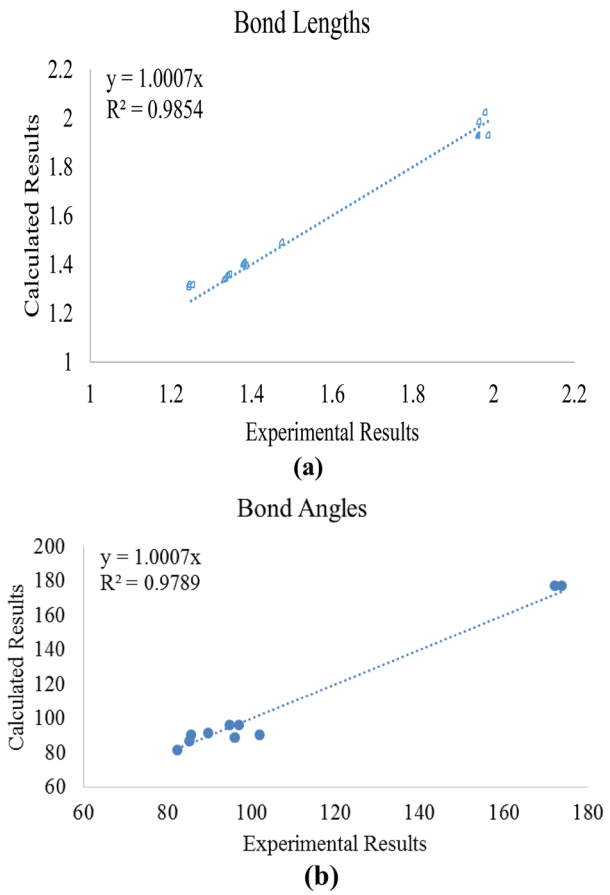

Fig. 10 The scatter graphs obtained from the experimental and calculated results for **a** bond lengths and **b** bond angles

Table 6 Experimental and calculated FTIR frequencies (cm^{-1}) obtained at the same level of theory in gas phase

Experimental	Calculated	Assignment
3500	3711	ν(OH)
3150	3074	ν_{as}(CH)
3100	3057	ν_{s}(CH)
1634	1677	ν_{as}(CO)
1599	1623	ν(C–C)
1560	1591	ν(C–N)
1335	1326	ν_{s}(C–O)
825	822	δ(O–C–O)
770, 729	798, 786	δ(CH)
445–553	375–561	ν(CuO)/ν(CuN)

Quantum chemical investigation

$[Cu_2(Bipy)_2(H_2O)_2(C_2O_4)(NO_3)_2]$ was optimized at HF method with LANL2DZ basis set in vacuum. The optimized structure is represented in Fig. 9. The relevant experimental and calculated structural parameters of the title compound are given in Table 5.

The distorted octahedral geometry of the copper complex is further confirmed by the calculated structural parameters given in Table 5. The scatter graphs are plotted for bond lengths and bond angles by using both experimental and calculated results, and are represented in Fig. 10. The correlation coefficient (R^2) and the equation of the graph were then calculated.

These results show a good correlation implying that the experimental geometric parameters agree well with the calculated ones. The calculated correlation coefficients values are, respectively, 0.9854 and 0.9789 for bond lengths and bond angles. In addition, the gradients of graphs are too close to one.

The IR spectrum is calculated at HF/LANL2DZ level in gas phase, and some frequencies with their assignments are given in Table 6. The calculated absorption vibrations are in agreement with the experimental results.

The molecular electrostatic potential map (MEP) and its contour are calculated for the title complex and represented in Fig. 11, which displays red regions in the environment of the oxygen atoms in the MEP map (Fig. 11.a). These regions are known as nucleophilic areas. The electron density is higher in this region than in the other regions. If this molecule interacts with any species, red regions will be active in these interactions.

Furthermore, ^{1}H and ^{13}C-NMR are calculated and given in Table 7, which shows chemical shift values of aromatic carbon atoms calculated in the range of 123–170 ppm. However, the oxalate carbon atoms should appear at 197 ppm. As for the hydrogen atoms, chemical shift values of the hydrogens in the aromatic rings are calculated in the range of 8–11 ppm. However, chemical shifts of the coordinated water hydrogens are calculated at 1.50 and 1.87 ppm.

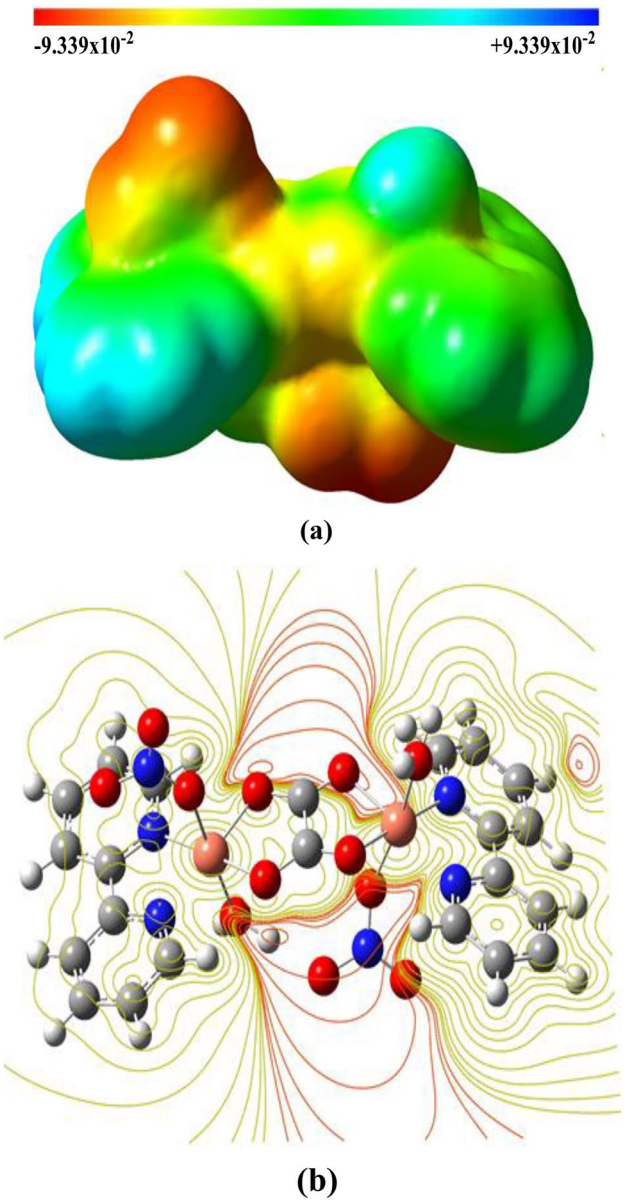

Fig. 11 **a** MEP map and **b** MEP contour of the studied complex at the HF/LANL2DZ level in gas phase

Table 7 Calculated chemical shift values (ppm) of carbon and hydrogen atoms in the NMR spectra

Assignments	^{13}C-NMR	Assignments	^{1}H-NMR
C1	163.38	C1–H1	10.48
C2	130.46	C2–H2	8.17
C3	146.52	C3–H3	8.70
C4	123.86	C4–H4	8.69
C5	167.54	C7–H7	8.75
C6	169.03	C8–H8	8.73
C7	124.26	C9–H9	8.18
C8	146.82	C10–H10	10.87
C9	129.82	O3–H1O	1.50
C10	164.46	O3–H2O	1.87
C11	196.95		

Conclusion

An oxalato-bridged dinuclear copper(II) complex based on 2,2′-bipyridine ligand has been prepared and fully characterized. The crystal structure and spectroscopic data revealed further insights into molecular copper(II) oxalate systems. The *Hirshfeld* surface analysis showed that the crystal structure is maintained by strong O–H…O, N–H…O and C–H…O hydrogen bonds, in addition to the weak C–H…π, π…π, π…*lp*/*lp*…π and *lp* …*lp* interactions. The quantum chemical calculations performed using HF/LANL2DZ levels indicated a good agreement between the calculated and experimental geometric structural parameter values and FTIR absorption vibrations. Moreover, the ^{1}H, ^{13}C-NMR spectra, the MEP maps and the MEP contours were calculated, examined in detail and the nucleophilic regions determined.

Acknowledgements The numerical calculations reported in this paper were performed at TUBITAK ULAKBIM, High Performance and Grid Computing Center (TRUBA Resources). AD acknowledges "The University of Abbes Laghrour Khenchela, Algeria" for financial support.

References

1. O. Kahn, *Molecular Magnetism* (Wiley-VCH, New York, 1993). **(and references therein)**
2. O. Kahn, Struct. Bond. **68**, 89–167 (1987)
3. H. Ojima, K. Nonoyama, Coord. Chem. Rev. **92**, 85–111 (1988)
4. J. Świątek-Kozłowska, I.O. Fritsky, A. Dobosz, A. Karaczyn, N.M. Dudarenko, T. Yu Sliva, E. Gumienna-Kontecka, L. Jerzykiewicz, J. Chem. Soc. Dalton Trans. **22**, 4064–4068 (2000)
5. M. Nonoyama, H. Ojima, K. Ohki, K. Nonoyama, Inorg. Chim. Acta **41**, 155–159 (1980)
6. O. Castillo, A. Luque, F. Lloret, P. Romàn, Inorg. Chem. Commun. **4**, 350–353 (2001)
7. D.Y. Naumov, A.V. Virovets, N.V. Podberezskaya, E.V. Boldyreva, Acta Cryst. **C51**, 60–62 (1995)
8. T. Bataille, D. Louër, Acta Cryst. **C55**, 1760–1762 (1999)
9. K.P. Strotmeyer, I.O. Fritsky, R. Ott, H. Pritzkow, R. Krämer, Supramol. Chem. **15**, 529–547 (2003)
10. S.V. Tomyn, E. Gumienna-Kontecka, I.O. Fritsky, T.S. Iskenderov, J. Świątek-Kozłowska, Acta Cryst. **E63**, m438–m440 (2007)
11. O. Castillo, I. Muga, A. Luque, J.M. Gutiérrez-Zorrilla, J. Sertucha, P. Vitoria, P. Roman, Polyhedron **18**, 1235–1245 (1999)
12. Oxford Diffraction. Oxford Diffraction Ltd., Xcalibur CCD system, CrysAlis Software system, Version 1.171 (2005)
13. M.C. Burla, R. Caliandro, M. Camalli, B. Carrozzini, G.L. Cascarano, L. De Caro, C. Giacovazzo, G. Polidori, R. Spagna, J. Appl. Cryst. **38**, 381–388 (2005)
14. G.M. Sheldrick, Acta Cryst. **C71**, 3–8 (2015)
15. L.J. Farrugia, J. Appl. WinGX Cryst. **45**, 849–854 (2012)
16. L.J. Farrugia, J. Appl. Cryst. **45**, 849–854 (2012)
17. I.J. Bruno, J.C. Cole, P.R. Edgington, M. Kessler, C.F. Macrae, P. McCabe, J. Pearson, R. Taylor, Acta Cryst. **B58**, 389–397 (2002)
18. A.L. Spek, Acta Cryst. **D65**, 148–155 (2009)
19. GaussView, Version 5, R. Dennington, T. Keith, J. Millam, Semichem Inc., Shawnee Mission, KS (2009)
20. Gaussian 09, Revision A.02, M.J. Frisch, G.W. Trucks, H.B. Schlegel, G.E. Scuseria, M.A. Robb, J.R. Cheeseman, G. Scalmani, V. Barone, B. Mennucci, G.A. Petersson, H. Nakatsuji, M. Caricato, X. Li, H.P. Hratchian, A.F. Izmaylov, J. Bloino, G. Zheng, J.L. Sonnenberg, M. Hada, M. Ehara, K. Toyota, R. Fukuda, J. Hasegawa, M. Ishida, T. Nakajima, Y. Honda, O. Kitao, H. Nakai, T. Vreven, J.A. Montgomery, Jr., J.E. Peralta, F. Ogliaro, M. Bearpark, J.J. Heyd, E. Brothers, K.N. Kudin, V.N. Staroverov, R. Kobayashi, J. Normand, K. Raghavachari, A. Rendell, J.C. Burant, S.S. Iyengar, J. Tomasi, M. Cossi, N. Rega, J.M. Millam, M. Klene, J.E. Knox, J.B. Cross, V. Bakken, C. Adamo, J. Jaramillo, R. Gomperts, R.E. Stratmann, O. Yazyev, A.J. Austin, R. Cammi, C. Pomelli, J.W. Ochterski, R.L. Martin, K. Morokuma, V.G. Zakrzewski, G.A. Voth, P. Salvador, J.J. Dannenberg, S. Dapprich, A.D. Daniels, Ö. Farkas, J.B. Foresman, J.V. Ortiz, J. Cioslowski, D.J. Fox, Gaussian, Inc., Wallingford CT (2009)
21. PerkinElmer, ChemBioDraw Ultra Version (13.0.0.3015), Cambridge Soft Waltham, MA, USA (2012)
22. Z. Zaim, T. Alagöz Sayin, K. Sayin, D. Karakaş, Turkish Comp. Theo. Chem (TC&TC) **2**(2), 7 (2018)
23. G. Kaştaş, Ç. Albayrak Kaştaş, A. Mhiri, F. Krichen, A. Oueslati, J. Lhoste, F. Goutenoire, M. Gargouri, A. Bulou, J. Alloys Compd. **772**, 546 (2019)
24. A. Günsel, E. Kırbaç, B. Tüzün, A. Erdoğmuş, A.T. Bilgiçli, M.N. Yarasir, J. Mol. Struct. **1180**, 127 (2019)
25. A. Echeverri, T. Gomez, C.Z. Hadad, Molecular Catalysis **471**, 9 (2019)
26. F. Gao, C.X. Yin, P. Yang, Chin. Sci. Bull. **49**, 1667–1680 (2004)
27. S. Kitagawa, T. Okubo, S. Kawata, M. Kondo, M. Katada, H. Kobayashi, Inorg. Chem. **34**, 4790–4796 (1995)
28. F.Q. Liu, Q.X. Wang, K. Jiao, F.F. Jian, G.Y. Liu, R.X. Li, Inorg. Chim. Acta **359**, 1524–1530 (2006)
29. S. Satyanaryana, J.C. Daborusak, J.B. Chaires, Biochemistry **32**, 2573–2584 (1993)
30. M. Julve, M. Verdaguer, O. Kahn, A. Gleizes, O. Philoche-Levisalles, Inorg. Chem. **22**, 368 (1983)
31. D. Kumar, I.P.S. Kapoor, G. Singh, R. Fröhlich, Thermochim. Acta **545**, 67–74 (2012)
32. A.N. Boyko, M. Haukka, I.A. Golenya, S.V. Pavlova, N.I. Usenko, Acta Cryst. **E66**, m1101–m1102 (2010)
33. P. Sun, S. Liu, D. Feng, F. Ma, W. Zhang, Y. Ren, J. Cao, J. Mol. Struc. **968**, 89–92 (2010)
34. R. Krämer, I.O. Fritsky, Eur. J. Org. Chem. **2000**, 3505–3510 (2000)

35. L. Kovbasyuk, H. Pritzkow, R. Krämer, I. O. Fritsky, Chem. Commun. **7**, 880–881 (2004)
36. Y.S. Moroz, L. Szyrweil, S. Demeshko, H. Kozłowski, F. Meyer, I.O. Fritsky, Inorg. Chem. **49**, 4750–4752 (2010)
37. J. Bernstein, R.E. Davis, L. Shimoni, N.-L. Chang, Angew. Chem. Int. Ed. Engl. **34**, 1555–1573 (1995)
38. S.C. Manna, J. Ribas, E. Zangrando, N.R. Chaudhuri, Inorg. Chim. Acta **360**, 2589–2597 (2007)
39. M.A. Spackman, P.G. Byrom, Chem. Phys. Lett. **267**, 215–220 (1997)
40. M.A. Spackman, D. Jayatilaka, Cryst. Eng. Comm. **11**, 19–32 (2009)
41. J.J. McKinnon, M.A. Spackman, A.S. Mitchell, Acta Cryst. **B60**, 627–668 (2004)
42. M. Spackman, J.J. McKinnon, Cryst. Eng. Comm. **4**, 378–392 (2002)
43. S.K. Wolff, D.J. Grimwood, J.J. McKinnon, M.J. Turner, D. Jayatilaka, M.A. Spackman, *Crystal Explorer* (University of Western Australia, Perth, 2012)
44. R. Vicente, A. Escuer, J. Ferretjans, H. Stoeckli-Evans, X. Solans, M. Font-Bardıá, J. Chem. Soc. Dalton Trans. 167–172 (1997)
45. L. Zhang, W.-M. Bu, S.-P. Yan, Z.-H. Jiang, D.-Z. Liao, G.-L. Wang, Polyhedron **19**, 1105–1110 (2000)
46. M.L. Calatayud, I. Castro, J. Sletten, F. Lloret, M. Julve, Inorg. Chim. Acta **846**, 300–302 (2000)
47. A. Gleizes, M. Julve, M. Verdaguer, J.A. Real, J. Faus, X. Solons, J. Chem. Soc. Dalton Trans. **2**, 3209–3216 (1992)
48. A. Bencini, A. Bianchi, E. Garcia-Espana, Y. Jeannin, M. Julve, M. Marcelino, M. Philoche-Levisalles, Inorg. Chem. **29**, 963–970 (1990)
49. A.K. Boudalis, V. Nastopoulos, S.P. Perlepes, C.P. Raptopoulou, A. Terzis, Transition Met. Chem. **26**, 276–281 (2001)
50. K. Nakamoto, Coordination Compounds. In Infrared and Raman Spectra of Inorganic and Coordination Compounds, 4th Ed., Wiley: New York (1986)